Influence of polymerisation parameters on the electro-optical properties of polymer-stabilised liquid crystals for smart glass application

C. Mahyaoui, F. Mondiot, Ivan Dozov, Patrick Davidson, C. Meyer

Taylor & Francis Word Template for journal articles

C. N. Mahyaoui[a]*, F. Mondiot[a], I. Dozov[b], P. Davidson[b], and C. Meyer[c]

[a]*Surface du Verre et Interfaces, Saint Gobain/CNRS, Aubervilliers, France;* [b]*Laboratoire de Physique des Solides, Université Paris Saclay, CNRS, Orsay, France;* [c]*Physique des Systèmes Complexes, Université de Picardie Jules Verne, Amiens, France.*

**camille.mahyaoui@saint-gobain.com*

Influence of polymerisation parameters on the electro-optical properties of polymer-stabilised liquid crystals for smart glass application

Smart windows are an important application of liquid crystal/polymer nanocomposites. Recently, an original design has been proposed for a window that switches from a scattering to a transparent state under an electric field. By polymerisation, the topological defects of the smectic A phase under hybrid anchoring conditions are stabilised in the nematic phase, making them addressable by the field. Here, we report the impact of the polymerisation parameters on the electro-optical properties and microstructure of the nanocomposites. We have first estimated the polymerisation kinetics and then investigated the influence of the UV-light intensity, monomer concentration, and photoinitiator concentration. UV-light intensity has little effect on the electro-optical properties of the device, although microstructural changes were observed. The monomer concentration has a strong impact on the scattering power in both the on- and off-states. A model is proposed to describe the dependence of the response times on the monomer concentration. Finally, no influence of the photoinitiator concentration on the electro-optical properties was observed. Polymerisation could occur even in the absence of photoinitiator, possibly due to the presence of impurities that could generate radicals under irradiation. Our study should help optimising the formulation of polymer-stabilised liquid crystal nanocomposites for industrial applications.

Keywords: smectic A, nematic, polymer, focal conic domains, optimisation, smart glass, PSLC

Introduction

Mixing polymers and liquid crystals (LCs) for electro-optical applications is a classic topic in LC science. In the late 1980's, the first prototype of a smart window based on

polymer dispersed liquid crystals (PDLCs), consisting of nematic droplets dispersed in a polymer matrix, was reported[1]. In PDLCs, the amount of liquid crystal usually does not exceed 30 wt%[2]. The device, which can switch from a scattering state to a transparent state, is presently available on the market with for example the product PRIVA-LITE®. In the early 1990's, a new type of smart window based on polymer stabilised liquid crystals (PSLCs) appeared[3]. This time, the liquid crystal is the main component of the system (typically between 90 and 99 wt%) and the polymer forms a mesh that traps and shapes the liquid crystal[4]. The polymer is usually obtained by photopolymerisation of acrylate monomers[5]. The main advantage of this type of device is that the transparent state is clear even for light rays impinging on the surface away from normal incidence, which is the main drawback of PDLC smart windows[6].

Since the 1990's, many types of devices based on PSLCs have been developed for electro-optical applications such as polymerised cholesterics for electrically switchable mirrors[7,8] and diffraction gratings[9], polymerised twisted and supertwisted nematics for low response times[10], and polymerised smectic A focal conic domains for adjustable lenses[11] and pixels[12]. Many types of smart windows have also been developed such as polymerised aligned nematics[3], polymerised cholesterics in different configurations[6,13–15], polymerised nematics with negative anisotropy of dielectric constant[16], and polymerised focal conic domains[17].

Many experimental studies have sought to better understand the polymer network / liquid crystal interaction and to identify the key control parameters. It has been shown that mesogenic monomers with flexible chains retain the director configuration better because they form fibres parallel to the director during polymerisation[18,19]. The 1,4-bis-[4-(3-acryloyloxypropyloxy)benzoyloxy]-2-methylbenzene (shown in Figure 2, also called ST03021, RM257 or C6M according to the supplier) is the most suitable and widely used

monomer for the formulation of PSLC systems[9,19,20]. The polymer network has been studied by scanning electron microscope (SEM)[4,5], electro-optical measurements[4,5], dynamic light scattering (DLS)[21], and neutron scattering[22,23]. Based on these data, several models have been developed to describe the polymer / liquid crystal interactions. Fung et al.[24] adapted the Landau-De Gennes theory to explain residual birefringence data and could deduce the diameter of the polymer fibres. The model of Kraig et al.[25] could predict the shift of the nematic-isotropic transition temperature as a function of the monomer concentration. Kossyrev et al.[26] and Yeng et al.[27] proposed models to explain the evolution of the Fréedericksz threshold and the decay time as a function of monomer concentration. All these models propose a description of the system at a submicron scale. The effects of the monomer concentration, UV power, photoinitiator concentration, UV exposure time, and polymerisation temperature on many PSLC systems have been extensively studied and reviewed by Dierking[5] and Broer, Crawford and Zumer[28].

The PSLC system studied here was first described in an article by Boniello et al. and was developed for smart window applications[17,29]. The idea is to combine the scattering power of defects generated in the smectic A phase (focal conic domains, FCD) and the reversible alignment transition that is induced by an electric field in the nematic phase. FCDs are defects that are often observed in layered liquid crystals (smectic, cholesteric, twist-bend nematic phases…) under hybrid (planar/homeotropic) anchoring conditions. The FCD structure can be described geometrically in terms of the "Cyclides de Dupin" as the layers bend and wrap around a hyperbola and an ellipse[30]. The precise structure of the layers in the case of 8CB coatings under hybrid conditions has been previously studied[31,32] and a schematic representation of the smectic layers is shown in Figure 1.

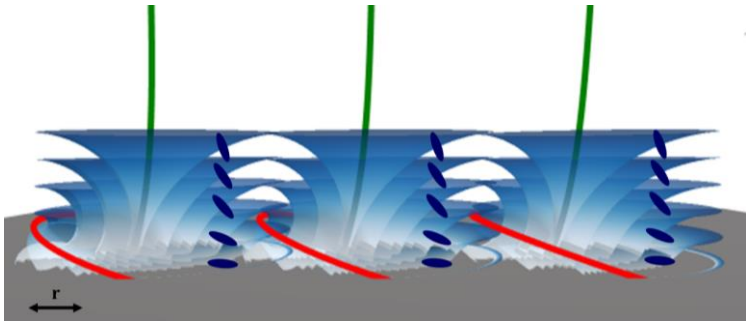

Figure 1: Representation of three focal conic domains. This type of defect is notably observed in the smectic A phase for liquid crystal coatings under hybrid conditions. The smectic layers (blue surfaces) bend and wrap around two singular lines: an ellipse (red line) and a confocal hyperbola (green line). The liquid crystal molecules are oriented perpendicular to the layers (dark blue ellipsoids). The rubbing axis is symbolised by the black double-headed arrow.

On the one hand, FCDs are interesting for smart window applications because they scatter light, but on the other hand, the nematic phase is desirable because it is easily addressed by applying an electric field. However, FCDs are not observed in the nematic phase because its structure is not layered. To induce FCDs in the nematic phase, Boniello et al, first generated FCDs in the smectic A phase, then they polymerised the system using small amounts of monomer (2 wt%). The polymer network freezes the structure of the defects, which remain in the nematic phase.

In this work, we systematically investigate the effects of different polymerisation parameters (kinetics, UV power, monomer, and photoinitiator concentrations) on the optical textures, electro-optical properties, and the morphology of the polymer network. We find the optimal values of these parameters not only with respect to smart window applications but also, more generally, for the most efficient use of PSLCs in electro-optical devices.

Material and methods

Sample preparation

The following chemicals were used as supplied: 8CB (4-octyl-4'-cyanobiphenyl, CAS number: 52709-84-9, Tokyo Chemical Industry, Figure 2.a), 5CB (4-cyano-4'-n-pentylbiphenyl, CAS number: 40817-08-1, Synthon Chemicals, Figure 2.b), ST03021 (1,4-bis-[4-(3-acryloyloxypropyloxy)benzoyloxy]-2-methylbenzene, CAS number: 174063-87-7, Synthon Chemicals, Figure 2.c), DMPA (2,2-dimethoxy-2-phenylacetophenone, CAS number: 24650-42-8, Tokyo Chemical Industry, Figure 2.d).

In a typical sample preparation, an 8CB/5CB (80/20 wt%) mixture was first prepared to lower the temperature of the smectic A / nematic transition below room temperature. Small amounts of monomer (ST03021) and photoinitiator (DMPA) were then added. Note that the photoinitiator mass fraction mentioned in this article are always expressed relative to the monomer mass fraction. The chemical formulas of the compounds are given in Figure 2 and the compositions of the samples are given in Table 1.

The mixture was introduced by capillarity into an 8 µm thick hybrid LC cell (S100A080uHAN, INSTEC, Co, USA) in the isotropic phase (50°C). The temperature was then lowered at 1°C/min to 5°C to reach the smectic A phase where a lattice of focal conic domains was formed. This temperature was chosen far enough away from the

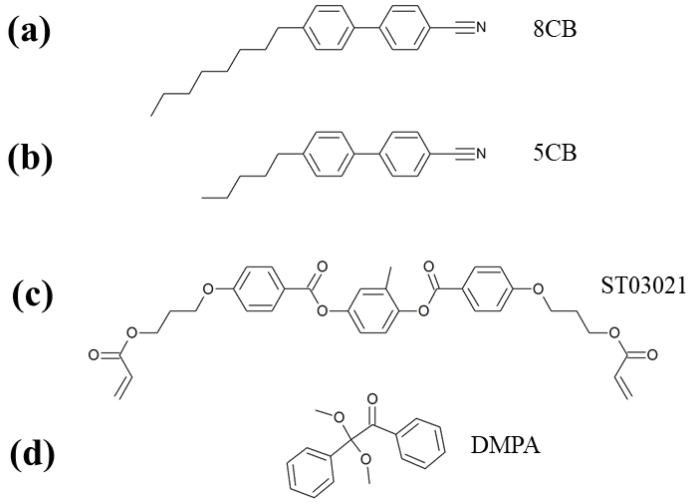

Figure 3: (a) 4-octyl-4'-cyanobiphenyl (8CB) (b) 4-cyano-4'-n-pentylbiphenyl (5CB) (c) 1,4-bis-[4-(3-acryloyloxypropyloxy)benzoyloxy]-2-methylbenzene (ST03021) (d) 2,2-dimethoxy-2-phenylacetophenone (DMPA)

nematic/smectic A transition temperature (which is around 16°C) to ensure that there is no phase transition during polymerisation due to the heat generated by this type of exothermic reaction. The sample was then exposed to UV light (365 nm, UV lamp Omnicure LX180, Lumen Dynamics) for 10 minutes to complete the polymerisation process. This exposure time was determined from a Raman study of the polymerisation kinetics. The UV light intensity was adjusted by varying the intensity of the UV power source and the distance between the source and the sample. Three series of samples were prepared to study the influence of different parameters (Table 1).

Table 1: Parameters used in the optimisation process.

	Series 1 Variation of UV light intensity	***Series 2*** Variation of monomer concentration	***Series 3*** Variation of photoinitiator concentration
UV power (mW/cm^2)	0.349 - 1.35 - 2.32 - 3.65 - 16.5 - 123 - 366	16.5	16.5
Monomer concentration (wt%, compared to the liquid crystal mass)	1.94	0.10 - 0.20 - 0.50 - 1.04 - 1.94 - 4.82 - 10.10 - 15.69	1.98
Photoinitiator mass fraction (wt%, relative to the monomer mass)	2.0	2.0	0.10 - 0.50 - 1.00 - 2.00 - 5.00 - 10.00 - 25.00 - 50.00

Sample characterisation

Raman measurements were performed using a confocal Raman microscope (inVia Qontor, Renishaw, circularly polarised laser, laser wavelength: 532 nm, objective 50X, laser power: 50 mW). The monomer was dissolved in toluene and 1 wt% of photoinitiator relative to the monomer mass was added. The mixture was introduced by capillarity into a 50 µm thick optical capillary and sealed with Canada Balsam. The samples were then exposed to UV light for different exposure times and the UV light intensity was set at 6.9 mW/cm^2.

The phase transitions of the pure compounds and their mixtures were characterised by differential scanning calorimetry (DSC Discovery, TA Instruments), using heating-cooling-heating ramps at 2°C/min.

The optical textures of the samples were observed using a polarising optical microscope (POM, Nikon Eclipse LV100N POL, Japan), between crossed polarisers, with a 20X objective (Nikon, NA: 0.40, WD 19 mm) equipped with a heating stage (LTS 420E, Linkam).

Sinusoidal AC voltages (f = 1 kHz) were applied to the samples in LC cells using a power supply (ITECH IT-M7700, MB Electronique).

Decay times were measured after applying 50 ms bursts of sinusoidal voltage (f = 100 kHz) to the sample. The optical response of the sample was observed without polariser, with the analyser perpendicular to the rubbing axis. The electro-optical signal detected by a photomultiplier tube mounted on the microscope (Leitz Ortholux) was accumulated by a digital oscilloscope (DSO-X 2004A, Keysight). A small load resistor (1 kΩ) was used to achieve a sub-microsecond response time of the setup.

Haze measurements were made using a spectrophotometer with an integrating sphere (Lambda950, PerkinElmer). For each sample, a spectrum of the total transmission [380 nm – 780 nm] and a spectrum of the diffuse transmission [380 nm – 780 nm] (light transmitted excluding a cone of 5° angle) were recorded. Haze is defined as the ratio of the diffuse transmission to the total transmission, integrated between 380 nm and 780 nm.

The microstructure of the samples was characterised by atomic force microscopy (AFM, ICON, Bruker, tapping mode).

To avoid destroying the polymer network when opening the cell, an alternative preparation method was developed. A polyvinyl alcohol (PVA, Mowiol® 4-98, CAS number: 9002-89-5) layer was deposited on a glass substrate and rubbed (Bench Top

Rubbing Machine, model: HO-IAD-BTR-01, Holmarc). A mixture of liquid crystals, polymer, photoinitiator and toluene was then spin-coated onto the PVA layer. The spin-coater parameters were chosen to obtain coatings as homogeneous as possible and with a thickness as close as possible to that of the cell. We were able to produce homogeneous 5 µm thick samples by adjusting the viscosity of the mixture by setting the liquid crystal/toluene volume ratio to 0.90, the rotation speed to 1000 rpm (for 60 s), and the acceleration to 500 rpm/s. The PVA layer provides the planar anchoring and the air homeotropic anchoring. Polymerisation was carried out under the UV lamp, as described above, and in a nitrogen atmosphere. The thickness of the layers was measured with an optical profilometer (NewView 6000, Zygo). The liquid crystalline compounds of the mixtures were then washed out: 30 µL of toluene was deposited on the sample and then spin-coated to evacuate the liquid crystal dissolved in the toluene (4000 rpm, 1000 rpm/s, 60 s). The procedure was done twice to ensure that all the liquid crystal was washed out. The samples were then characterised by AFM. Note that because the polymerisation is carried in coatings and not in cells, the trends observed by AFM as the different parameters are varied (UV light intensity, monomer concentration, photoinitiator concentration) are not quantitatively comparable to the results obtained in cells. This could be due to the presence of traces of dioxygen, despite the nitrogen atmosphere.

The composition of 8CB, supplied by Tokyo Chemical Industry, was analysed by liquid chromatography coupled to high resolution mass spectrometry (LC-HRMS). A Dionex Ultimate 3000 LC instrument coupled with a Thermo Q-Exactive Orbitrap mass spectrometer was used. The LC column was a Hypersil C8 (ThermoFisher, 100 x 2.1 mm, 1.9 µm). A water – acetonitrile gradient was used in the LC column, both acidified with 0.1% of formic acid. The Q-Exactive system was equipped with a heated electrospray ionisation probe. MS spectra were recorded with positive ionisation in the 150 to 1500

m/z range. The resolution of the HRMS is 70 000 for m/z of 200. The UV-visible acquisition was made in the 200 – 800 nm range.

Results and Discussion

Polymerisation kinetics

Polymerisation times for PSLC reported in the literature vary from 3 minutes[33] to 5.5 hour[34]. Before varying the other polymerisation parameters (the UV power, monomer and photoinitiator concentrations), it was necessary to first select a UV-exposure time long enough to ensure that the polymerisation would be completed regardless of the values of the other parameters. Indeed, the polymerisation rate in the case of radical polymerisation (in the steady-state approximation) is given by[35]: $R_p = -\frac{d[M]}{dt} = \frac{k_p}{\sqrt{k_t}}[M]\sqrt{\phi I_0 \varepsilon [A]}$ where [M] is the monomer concentration, k_p is the propagation rate constant, k_t is the termination rate constant, Φ is the photoinitiator efficiency, I_0 is the incident light intensity, ε is the absorption coefficient of the photoinitiator, and [A] is the concentration in photoinitiator.

In order to evaluate the polymerisation kinetics under conditions as close as possible to those prevailing in the electro-optical cells, the conversion of the C=C bonds of the monomer was followed directly by confocal Raman microscopy. Indeed, as polymerisation proceeds, the C=C bonds are converted into C-C bonds (Figure 1SI). The C=C peak maximum is at 1637 cm^{-1} [36] and its area is proportional to the C=C concentration. The C=C peak area is normalised by the C=O peak area (maximum at 1735 cm^{-1} [36]) which should remain constant, allowing us to compare the kinetics at two monomer concentrations: 20 wt% and 30 wt%. Moreover, the monomer was dissolved in toluene instead of the 8CB/5CB mixture because the signal of the 8CB and 5CB aromatics

was too close to the C=C peak. It has been shown that the polymerisation rate depends on the liquid crystal phase: polymerisation is faster in the smectic phase than in the isotropic phase[37,38]. The reaction times that we will measure in toluene may be slightly overestimated, but we just want to determine the time needed to complete the reaction. The kinetics experiments were carried out with a monomer concentration much higher than that used in ordinary PSLCs (20 - 30 wt% instead of 1 wt% - 5 wt%) in order to obtain enough signal. We assumed the reaction kinetics to be first order, so that it does not depend on the monomer concentration. The toluene/monomer mixture was inserted

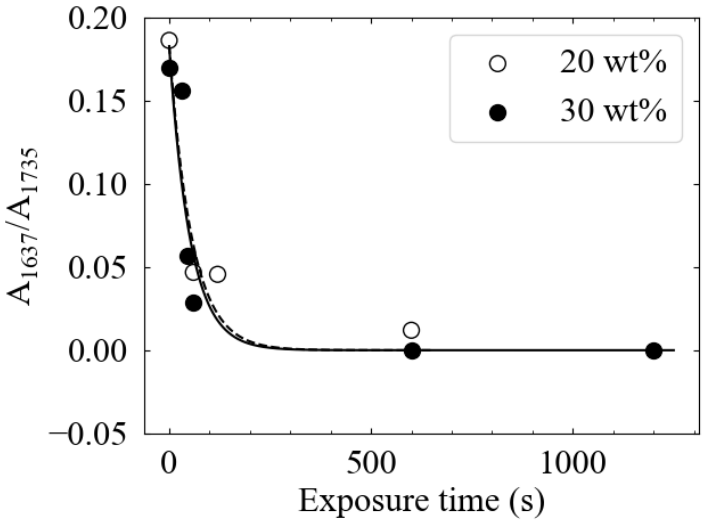

Figure 4: Polymerisation kinetics of S103021 in toluene at two concentrations (20 wt% and 30 wt%), as followed by Raman spectroscopy. Dependence of the ratio of the area of the peak at 1637 cm^{-1}(C=C) to that of the peak at 1735 cm^{-1} (C=O) versus UV exposure time. Lines: fits of the data by an exponential decay ($y(t)=y_0 * \exp(-t/B)$). The dotted line is the fit for 20 wt% of monomer and the solid line is the fit for 30 wt% of monomer. For 20 wt%, B= 56 s and for 30 wt%, B = 52 s.

into 50 µm thick glass capillaries and the capillaries were then sealed to avoid O_2 inhibition of the reaction. The capillary thickness was chosen to be small enough to ensure that the UV absorption was the same throughout the thickness of the sample[39].

The dependence of the ratio of peak areas on exposure time was fitted by an exponential law derived from eq (1): $y(t) = y_0 e^{-t/B}$ where y_0 is proportional to the initial $n_{C=C}/n_{C=O}$

ratio, y(t) is proportional to the $n_{C=C}/n_{C=O}$ ratio at time t and $B = 1/\frac{k_p}{\sqrt{k_t}}\sqrt{\Phi I_0 \varepsilon [A]}$. The kinetic constants k_p and k_t cannot be deduced from this fit but the reaction half-time can be expressed as: $t_{1/2} = \ln(2) \times B$, which should indeed not depend on the monomer concentration, due to the assumption of a first-order reaction.

As shown in Figure 3, the reaction half-time is around 39 s for 30 wt% monomer and around 36 s for 20 wt% monomer. The reaction half-time does not seem to depend much on the monomer concentration, confirming the first-order reaction hypothesis.

In usual photopolymerisation of acrylates, polymerisation is completed in a few seconds[40] or minutes[35], but here the monomer is extremely diluted (2 wt%) compared to classical polymerisation studies where the monomer is not dissolved in a solvent. For PSLC, it is therefore difficult to directly follow the monomer concentration and the conversion rate (evolution of the C=C bond concentration) because the monomer is extremely diluted (between 1 wt% and 10 wt%). Consequently, indirect techniques have been developed. Gu et al.[21] performed in situ time-resolved dynamic light scattering on PSLC and concluded that the reaction was completed 20 minutes after a 10-minute long UV irradiation. They fitted their data with an exponential decay, consistent with a first-order reaction, and found a rate constant of 0.1 min^{-1}. Guymon et al.[38] studied the polymerisation of PSLC by differential scanning calorimetry and found that the polymerisation was completed in approximately 100 s. Wall et al.[41] studied the polymerisation of PSLC (E7/monomer : 97/3 in mass) by FTIR and concluded that the reaction was completed in less than 10 minutes. Therefore, our results are in good agreement with those reported in the literature.

To ensure that the reaction is completed regardless of the photoinitiator concentration or UV light intensity, we set the polymerisation time to 10 minutes for the next experiments.

Influence of UV light intensity

The effect of UV light intensity was first investigated. For this purpose, the monomer concentration was set to 2 wt% with respect to the liquid crystal mass and the photoinitiator concentration to 2 wt% compared to the monomer mass. These values are standard according to the literature[5].

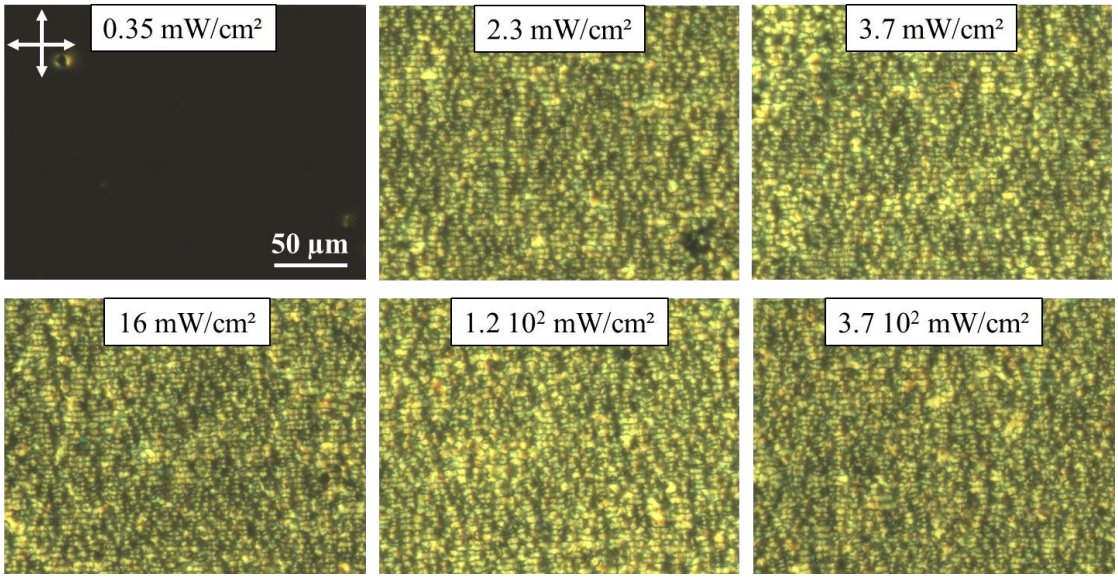

Figure 5: POM images of samples, between crossed polarisers (white cross), from series 1 (UV light intensity variation) after polymerisation, 25°C, nematic phase (no field applied).

The most direct, albeit qualitative, way of assessing the completion of the polymerisation is to examine the texture of the sample at room temperature (in the nematic phase, after the reaction) because the persistence of the focal conic defects of the smectic phase is a sign that the polymerisation is complete (Figure 4). Below a UV light intensity threshold (between 0.35 mW/cm² and 2.3 mW/cm²), focal conic domains are not observed and the nematic texture remains exactly as before polymerisation. Above this threshold, the smectic A defects are retained in the nematic phase and no significant evolution was observed with variation of the UV light intensity over two decades.

To our knowledge, the literature does not mention any UV light intensity threshold for the polymerisation reaction in the investigated range (from 0.01 mW/cm² [34] to 4 W/cm²

[24]). Besides, the minimum UV light intensity that we observed could depend on several experimental parameters, such as the efficiency of photoinitiator dissociation, the match between photoinitiator and UV lamp spectra, and the exposure time.

Since more quantitative measurements are required to detect any differences between the samples of series 1 (UV light intensity variation), their electro-optical properties were investigated. Haze measurements in the off- and on-states (0 V and 40 V) as a function of UV light intensity (Figure 5) confirm the existence of a threshold. Above this threshold, in good agreement with the POM observations, there are no differences between the samples in the off-state (0 V: "scattering state"). This simply suggests that, above the threshold, the UV power is high enough to initiate the polymerisation, which preserves the smectic defects.

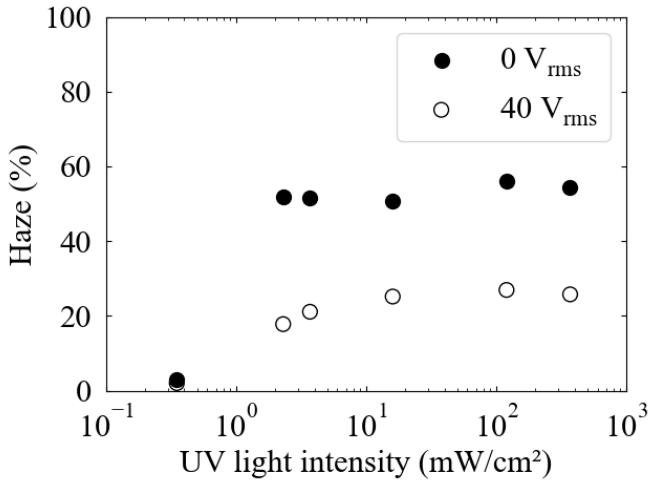

Figure 6: Haze measurements, at 0 V and 40 V, versus UV light intensity during the polymerisation process.

However, in the on-state (40 V: "transparent state"), a slight increase in haze is observed as the UV light intensity is increased. This could be due to an evolution of the morphology of the polymer network with UV light intensity.

The threshold appears again in the dependence on UV light intensity of the decay time, τ_{off}, of the samples, which drops from around 8 ms to around 2 ms when the UV light intensity is increased from 0.35 to 1.35 mW/cm^2 (Figure 6). We have checked (see Suppl. Info. Section 2 for details) that this is indeed due to the polymer network and not to a change in texture (distorted nematic vs focal conic domains).

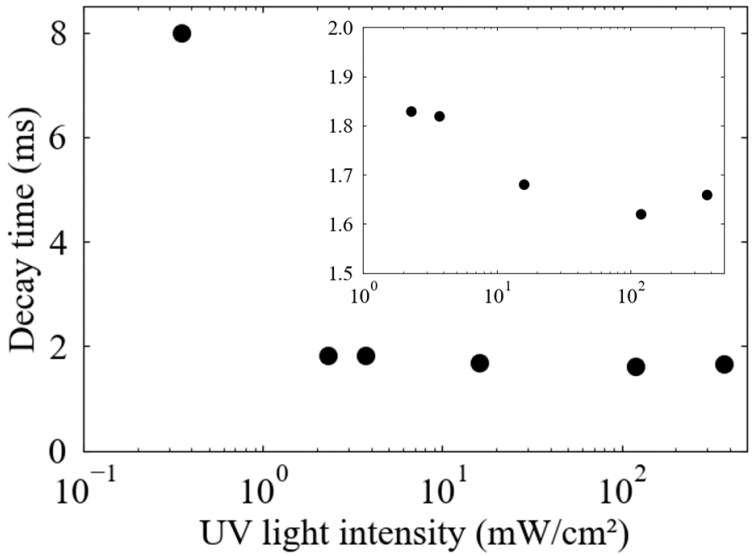

Figure 7: Dependence on the UV light intensity of the decay time of the electro-optical signal of the system after applying a voltage pulse (40 V_{rms}).

Note that, in most cases, the electro-optical curves showed two different decay times (Figure 2SI). We only considered the shortest one and fitted the corresponding part of the curve with a single exponential decay. This phenomenon has already been reported once in the literature using a different characterisation method[34].

A closer look at the dependence of the decay time on the UV power reveals the same trend as that of the haze at 40 V, and a linear correlation is found between these two quantities (Figure 7), which leads to two conclusions. Firstly, the small increase in haze, at 40 V (Figure 5) and the small decrease in decay time (Figure 6), observed above the UV light intensity threshold, are indeed significant because two independent

measurement techniques show the same trend. Secondly, as the UV light intensity is reduced, the decay time increases and the haze at 40 V decreases, indicating that the contact area between the polymer strands and the liquid crystal decreases. Thus, the anchoring effect of the polymer in the bulk on the liquid crystal becomes weaker, allowing the latter to align more easily along the field (low haze at high voltage) and increasing its relaxation time.

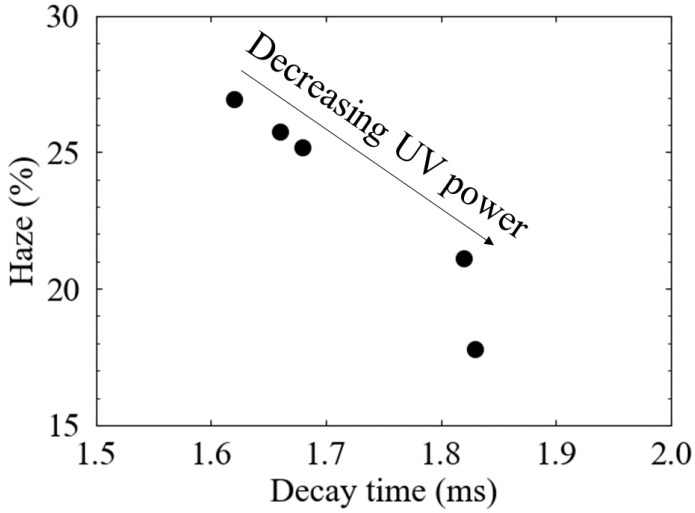

Figure 8: Haze at 40 V vs decay time at 40 V for samples of series 1 (UV light intensity variation).

The decrease in contact area between the polymer strands and the liquid crystal with decreasing UV light intensity could be due to two things. Firstly, the polymerisation rate increases with UV power[40] so if the UV-exposure time is too short, the reaction might not be completed for low UV light intensity and the polymer network might thus be less dense. However, the UV-exposure time was carefully chosen to ensure that the reaction was completed even for small UV light intensity, and this is confirmed by monitoring the SmA-N transition temperatures (Figure 3SI). This hypothesis can therefore be ruled out.

Secondly, the morphology of the polymer network could change as the UV light intensity is increased: at high UV light intensity, many radicals are generated simultaneously at the beginning of the reaction, so that the polymer network consists of many short polymer chains. It has been shown for acrylate polymerisation that the molecular weight fraction decreases and the polydispersity increases as the UV intensity increases[42]. The structure of our polymer network is different because it is organised by the liquid crystal matrix. We could imagine that as the UV intensity increases, the polymer fibres become shorter and more branched and thus more numerous, which would increase the contact area between the liquid crystal and the polymer. Microstructural analysis could help to shed some light on this issue.

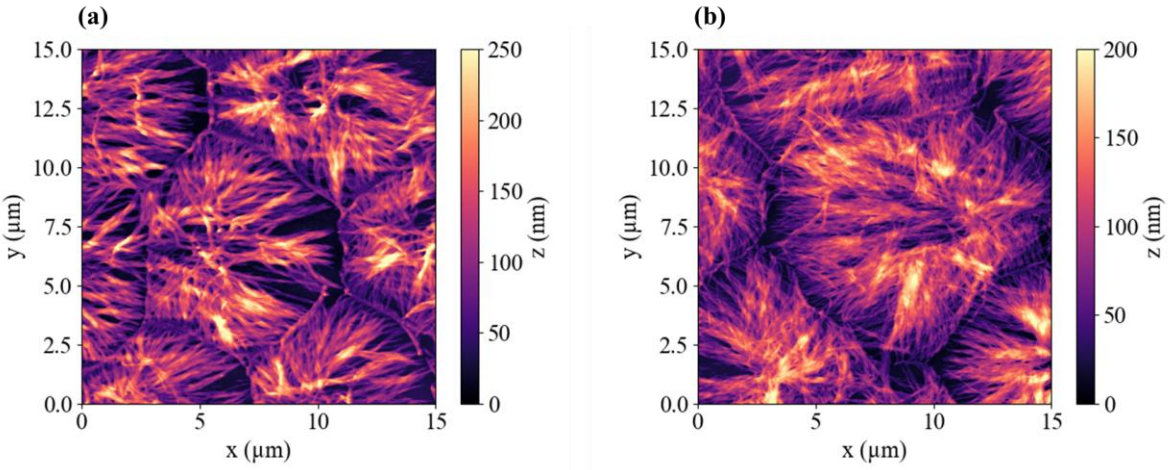

Figure 9: AFM height profiles of washed polymerised coatings. The applied UV light intensity was 16.5 mW/cm² in (a) and 366 mW/cm² in (b). In both cases, the reactive mixtures contained 2 wt% of monomer and 2 wt% of photoinitiator relative to the monomer mass.

An AFM study of coatings that closely replicate the systems in electro-optical cells (see Experimental section) provides clues to better understand Figures 5, 6, and 7. Figure 8 shows the height profile of the polymer network (after washing out the liquid crystal) of two samples differing only by the UV power applied (16.5 mW/cm² for Figure 8 (a) vs 366 mW/cm² for Figure 8 (b)).

Previous studies allow us to better understand these images. Firstly, the polymer fibres observed probably follow the director field during polymerisation[5,43]. These fibres are only observed with suitable monomers[19,33] and the morphology of the polymer network is often interpreted in terms of a phase separation process and the competition between the polymerisation reaction rate and the diffusion rate[18]. It has been shown that when the polymerisation takes place in the smectic A phase, the polymer strands orient perpendicularly to the smectic layers[19]. These AFM images thus provide a representation of the director field in a focal conic domain. Singular lines are particularly visible at the edges of each defect, which is the place where two fibre orientations meet. Some samples were also examined by SEM. Both a side view and a tilted view of the sample were taken to better assess the polymer network in three dimensions (Figure 4SI). These images show that the polymer network has collapsed due to the washing of the liquid crystal. Therefore, only the projection of the orientation of the fibres in the (x,y) plane parallel to the substrate can be reliably determined. Nevertheless, the SEM images are quite similar to the AFM images we have previously obtained and largely confirm the observations of Guymon et al and their claim that that the polymer strands are oriented perpendicular to the smectic layers[19]. To our knowledge, this type of images of the polymer network in polymerised focal conic domains, at the microscopic scale, has only been observed once in the twist-bend nematic phase[44] and with less detail. Therefore, this approach is a new tool to study the structure of FCDs.

Although the two images in Figure 8 are rather similar, the polymer network appears more branched in the case of the sample exposed to the highest UV light intensity. Ma et al.[45] also observed that as the UV intensity increases, the polymers became more branched and the diameter of the fibres decreased. This trend was also observed by Fung et al[43]. In our samples, we did not observe a significant variation in fibre diameter (Figure 5SI),

although the polymer network is clearly more branched at high UV light intensity. This suggests that the trend observed in Figure 7 is probably mainly due to a change in morphology, in agreement with the literature : Ma et al.[45] observed that the Fréedericksz threshold increased with UV light intensity and they attributed this effect to the increase in fibre diameter. Conversely, Dierking et al. investigated the effect of UV-light intensity on the electro-optical properties of polymerised cholesterics and observed a slight decrease in the threshold voltage as the light intensity increased. They also observed first a slight decrease of the decay time as the light intensity increased from 0.01 mW/cm² to 0.1 mW/cm² and then a sharp rise of the decay time as the light intensity increased to 10 mW/cm².

In the following, the UV light intensity was set to 16.5 mW/cm².

Influence of monomer concentration

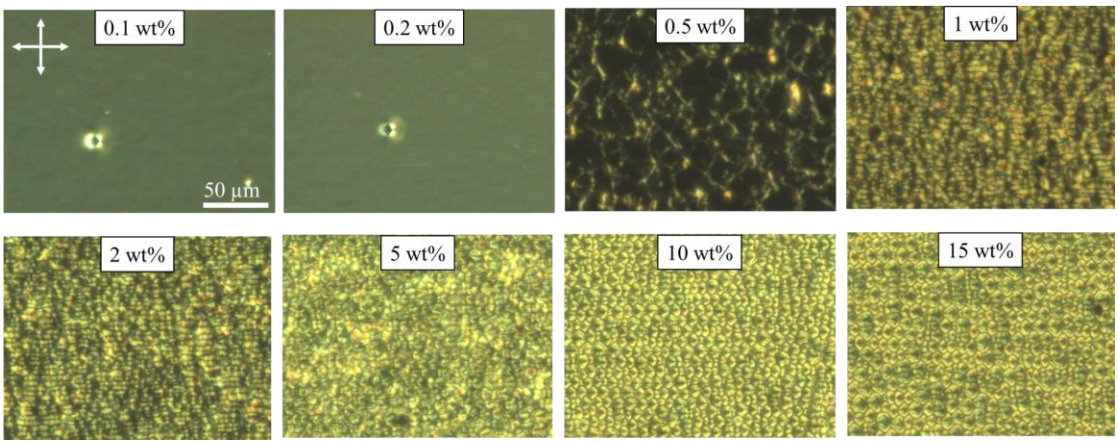

Figure 10: POM images of samples, between crossed polarisers (white cross), from series 2 (monomer concentration variation) after polymerisation, 25°C, nematic phase (no field applied).

The influence of the monomer concentration (series 2) was then investigated, keeping the photoinitiator concentration constant, at 2 wt% (relative to the monomer mass). The monomer mass fraction was varied between 0.1 wt% and 15 wt%, but above 5 wt%, we

couldn’t solubilise all the monomer crystalline powder in the liquid crystal, even if the flask was heated. When the cell was filled by capillarity, the undissolved crystals were too large to enter the cell. The cell looked homogeneous and no phase separation was observed before or after polymerisation. This solubility limit is in agreement with that reported in the literature[26]. The SmA-N transition temperatures were measured by optical microscopy and differential scanning calorimetry before and after polymerisation (Figure 6SI). Before polymerisation, the SmA-N transition temperature decreases with increasing monomer mass fraction. After polymerisation, the SmA-N transition temperature doesn’t depend on the monomer mass fraction anymore.

The optical textures observed in the nematic phase at room temperature after polymerisation (Figure 9) show that, below 0.5 wt% monomer, the focal conic domains of the smectic phase are not retained in the nematic phase. At 0.5 wt%, an intermediate state is obtained, with a texture that is no longer uniform, while above 0.5 wt%, the defects are maintained in the nematic phase thanks to the polymer network. Therefore, there seems to be a threshold monomer concentration of 0.5 wt% below which the polymer network formed is not dense enough to retain any smectic defects.

A similar evolution is expected for the haze measurements, both in the off-state (0 V) and in the on-state (40 V), as shown in Figure 10.

Indeed, at very low monomer concentrations (0.1 wt% and 0.2 wt%), no difference is observed between the off-state and the on-state. In fact, because there are no focal conic domains and very little polymer, the off-state does not scatter light. Moreover, when the electric field is applied, the liquid crystal aligns along the field, but since the transparency is already excellent, the field hardly affects it. Above the 0.5 wt% monomer concentration threshold, the haze of the samples increases with the monomer mass fraction, both at 0 V and 40 V.

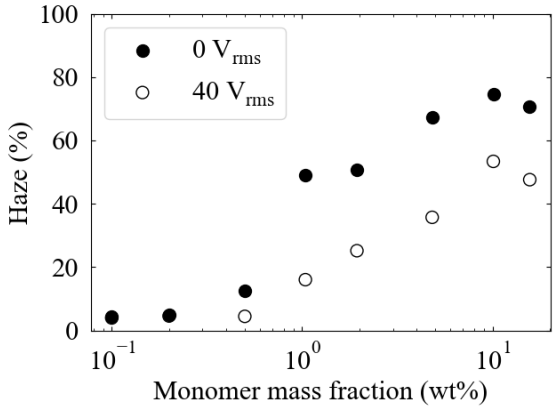

Figure 11: Dependence on the monomer concentration of the haze in the off-state (0 V) and the on-state (40 V).

A first possible explanation for this behaviour is based on the sample textures. As the monomer concentration increases, focal conic domains are better retained in the nematic phase and therefore better scatter light, hence the haze at 0 V increases. The defects are probably better maintained because the polymer network is denser and the surface contact between the polymer fibres and the liquid crystal is improved. Then, the polymer anchoring effect increases and alignment of the liquid crystal along the field becomes more and more difficult[16,46]. Even at high voltages, there are still areas of distorted director that scatter light, which explains why the haze at 40 V increases with the monomer concentration.

A second possible explanation is based on the contrast in refractive index between the liquid crystal and the monomer. The optical indices of liquid crystal and polymer systems,

taken from the literature, are shown in the supplementary information (Table SI1). Since there is a slight difference in refractive index between the liquid crystal and the polymer, then the latter could contribute to the light scattering, which would indeed increase with the amount of polymer. However, the index difference is very small, so it is neglected here.

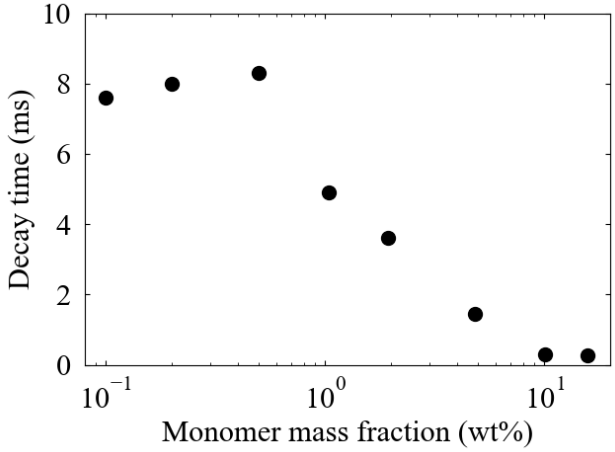

Figure 12: Decay time after a 40 V pulse versus monomer mass fraction (wt%) (series 2, monomer concentration variation).

As shown in Figure 11, the electro-optical decay time decreases with increasing monomer mass fraction above the 0.5 wt% threshold. The same trends have been observed with similar systems[3,26,47]. The typical evolution of the intensity as the field is switched off is shown in Figure SI7. Initially, the intensity decreases rapidly, following an approximately exponential law (Figure SI7, zone I). This part of the decay is qualitatively similar to the usual behaviour of a nematic cell, but is significantly faster. Indeed, the decay time depends on the characteristic lengths, ξ_n, of the excited distortion modes during the application of the field. In a cell with thickness d and strong anchoring on the boundary surfaces, $\xi_n = d/\left[\pi(2n+1)\right]$ with $n = 0, 1, 2, \ldots$, and the corresponding relaxation times are $\tau_n = \gamma_1 \xi_n^{\,2} / K$, where γ_1 is the rotational viscosity of the nematic and *K* is the

relevant elasticity constant. Due to the fast decrease of τ_n with the mode number *n*, the decay curve ends in a single-exponential regime, ~ exp(-t/τ_0), with $\tau_0 = \gamma_1 d^2 / (\pi^2 K)$. The much faster decay time, τ, of the polymerised cells reveals that the corresponding length ξ is much smaller, due to the anchoring of the nematic on the adjacent polymer fibres rather than on the much more distant boundaries of the cell.

After the usual approximately exponential part, the decay curve shows a plateau or a small bump, which is not present for the non-polymerised cell (Figure SI7 zone II). The low intensity and the much longer relaxation time of this signal indicate that it is related to the relaxation of the polymer fibre network on a larger scale. Indeed, due to the anchoring of the nematic on the fibres, the electrical torque is transmitted to the polymer structure and distorts it to some extent.

Here we focus only on the fast response of the nematic itself. This type of response has been theoretically analysed for polymer-stabilised cells with planar alignment and therefore with a much simpler geometry. The specificity of the decay response for a polymer-stabilised cell is due to the fact that the nematic is anchored on the neighbouring polymer fibres rather than on the boundary surfaces, i.e. the anchoring is “distributed” throughout the bulk of the cell. Two different approximations have been proposed to describe this anchoring, either on virtual polymer surfaces stacked in the cell[48] or on the faces of a rectangular unit cell formed by the polymer fibres[26]. In both cases, the cell undergoes a Fréedericksz transition with a much larger threshold and a faster response time than in a usual nematic cell without polymer stabilisation. In our case, however, the geometry of the cell is much more complex, as the fibres and the nematic itself are not planarly aligned (without a field), but are organised in focal-conic-like structures. Throughout the cell, the local director orientation varies and is, in general, tilted at an arbitrary angle with respect to the field. Due to this tilt, there is no a Fréedericksz

transition in the "unit cells", but a smooth realignment of the nematic director even at fields much weaker than the Fréedericksz threshold (Figure SI8). Moreover, the relation between the relaxation time of the "unit cell" and the experimentally measured optical relaxation time τ_{opt} is much more complex in our case: instead of the simple relation $\tau_{opt} = \tau_0/2$ for planarly oriented cells, in our geometry τ_{opt}/τ_0 is a function of the local tilt angle of the fibres, θ_0.

To qualitatively describe the decay behaviour of our polymer-stabilised cell, we consider a small region in which the polymer fibres with radius r_0 are tilted at an angle θ_0 with respect to the applied field **E** ‖ **z**, the normal to the cell. We assume that the fibres are approximately uniformly distributed in the cell, with an average separation of $2R_0$ (see Figure 12.a). Comparing the volumes of the polymer and nematic regions, we obtain $r_0 / R_0 = \sqrt{c}$, where c is the volume fraction of the polymer. As the densities of the polymer and the liquid crystal are close to 1, the monomer mass fraction c_m is assumed to be very close to c. In the remainder of this text, these two quantities are assumed to be equal. As a "unit cell", we consider a cylindrical region around each fibre, with $r_0 < r < R_0$. Without a field, the nematic is oriented parallel to the fibre due to its anchoring on the fibre surface (for simplicity, we assume that the anchoring is extremely strong). Under field, the nematic director rotates at some angle $\delta = \delta(r)$. The boundary conditions for $\delta(r)$ are $\delta(r_0) = 0$ and $d\delta/dr = 0$ at $r = R_0$ (see Figure 12.b). Therefore, $\delta(r)$ can be developed in Fourier series with generic term $\sin(\frac{2m+1}{2}\frac{\pi r}{R_0})$, m = 0,1,2,… The relaxation time of the m-th term is given by $\tau_m = \gamma_1 \xi_m{}^2 / K$, where $\xi_m = 2R_0 / \left[\pi(2m+1)\right]$ is the characteristic length of the corresponding relaxation mode. Similar to the case of the planar cell, the last part of the decay function relaxes as

exp(-t/τ_0), where $\tau_0 = 4\gamma_1 R_0^2/(\pi^2 K) = 4\gamma_1 r_0^2/(\pi^2 c K)$ is the characteristic time of the slowest relaxation mode. As τ_0 is independent of the orientation of the "unit cell", it will also be the decay time of the polymer-stabilised cell after averaging over all the fibre orientations. The corresponding optical relaxation time will be of the same order of magnitude, $\tau_{opt} = \tau_0 / a$, where $1 < a < 2$ is a numerical coefficient depending on the average tilt of the fibres in the cell.

Figure 11 shows the decay times measured in cells with the same thickness, d = 8 µm,

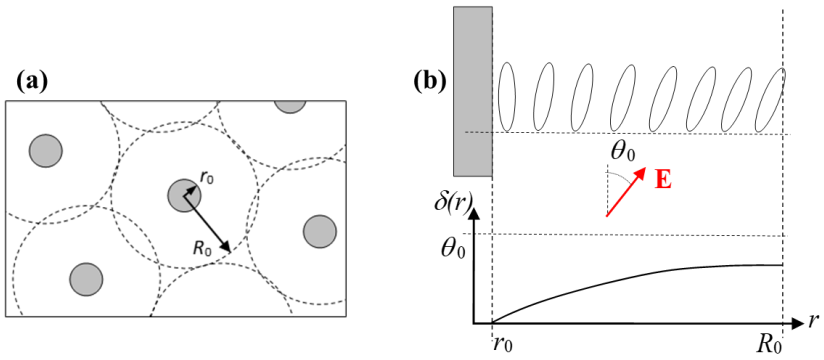

Figure 12: (a) The polymer fibres are modelled as cylinders of radius r_0 separated by $2R_0$. (b) Boundary conditions of the angle δ.

and different concentrations *c*, of polymer fibres. Up to about *c* = 0.5 wt%, the decay time remains the same as in the absence of polymer. At higher polymer content the decay time decreases rapidly, following approximately a c^{-1} law (see the fit in Figure 13). A comparison of this behaviour with our theoretical estimate of τ_0 indicates that the radius of the polymer fibres, r_0, is approximately independent of the concentration. The data τ_{opt} vs 1/c can be fitted with a linear function and the slope found is 4.5 10^{-5} s. Thanks to the expression $\tau_{opt} = 4\gamma_1 r_0^2/(\pi^2 cKa)$, we calculated the theoretical slope using standard values (γ_1=0.1 Pa.s[49], r_0=50 nm, K=5 pN[50,51], a=1) and found 2.0 10^{-5} s, which is of the same order of magnitude.

This analysis confirms previous literature reports that the decrease in decay time with increasing monomer mass fraction can be explained by a gradual compaction of the polymer network[16,52] and that if the polymer strand diameter remains constant[45,53], then the number of strands increases and thus the characteristic mesh size decreases.

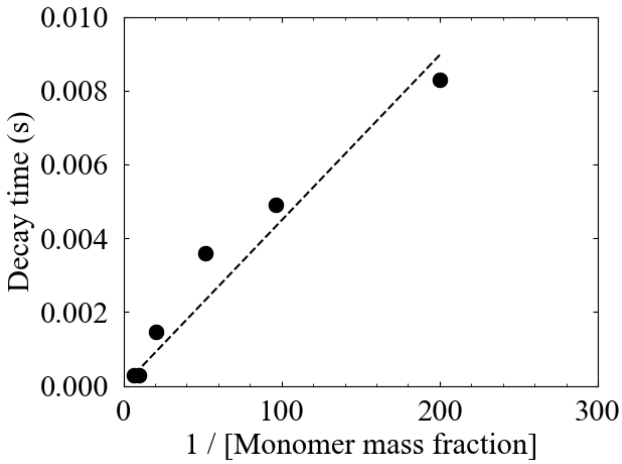

Figure 13: Approximation of τ_{opt} vs $1/c_m$ by a linear fit (c_m is the monomer mass fraction). Since the densities of the liquid crystal and the polymer are close to 1, the monomer mass fraction was used for the monomer volume fraction.

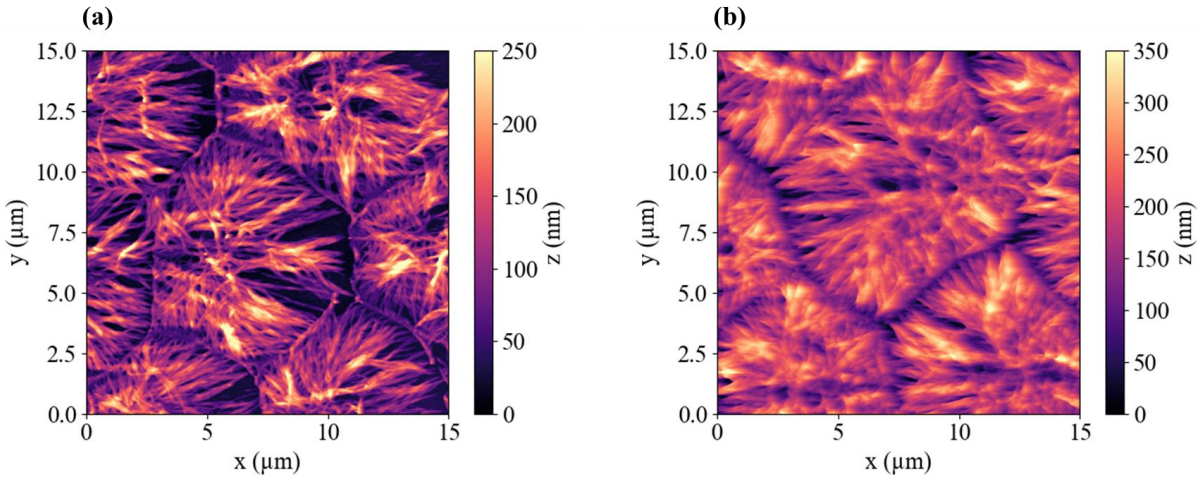

Figure 14: AFM height profiles of washed polymerised coatings. The monomer mass fraction is 2 wt% in (a) and 5 wt% in (b). In both cases, the reactive mixtures contained 2 wt% of photoinitiator relative to the monomer mass and the applied UV light intensity was 16.5 mW/cm².

AFM analyses were done to better support this explanation.

As shown in Figure 14, the diameter of the fibres does not change significantly with increasing monomer concentration, but there are many more fibres in the 5 wt% monomer sample than in the 2 wt% monomer sample. This effect was confirmed by SEM analyses of the same samples (Figure SI9). The effect of the monomer concentration on the morphology of the network has been studied extensively. When the diameter of the fibres was measured by fitting electro-optical curves, it was found that the diameter of the fibres decreased as the monomer concentration increased[45,54]. However, direct images of the polymer network obtained by SEM showed that the diameter of the fibres was independent of the monomer concentration[16,45,55]. Our results are consistent with this literature.

The polymer network also becomes denser with increasing monomer concentration, but the shape of the focal conic domains is still well defined. This supports our hypothesis mentioned above in the discussion of haze measurements that as the monomer concentration increases, the contact area between the liquid crystal and the fibres increases, making it more difficult to align the liquid crystal.

To conclude this section, the monomer concentration that gives the best compromise between a sufficiently scattering off-state and a sufficiently clear on-state is around 1-2 wt%.

Influence of the photoinitiator concentration

Finally, the effect of the photoinitiator concentration was studied, keeping the monomer concentration at 2 wt% and the UV power at 16.5 mW/cm². As little variation was observed over a wide range of photoinitiator concentrations (0.1 – 50 wt% relative to the monomer mass), a control sample without any photoinitiator was also prepared. The evolution of the SmA-N transition temperature shows that the polymerisation is complete for each sample (Figure SI10). The textures of the samples at room temperature (in the nematic phase) after polymerisation are shown in Figure 15.

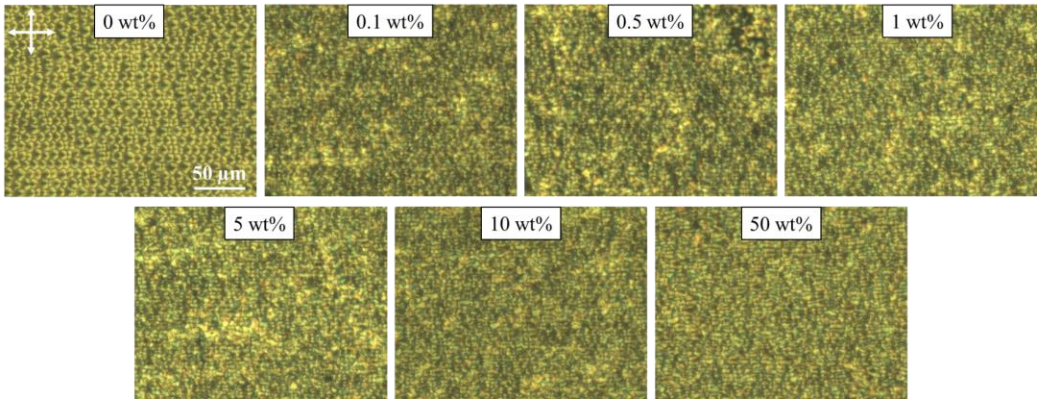

Figure 15: POM images of samples, between crossed polarisers (white cross), from series 3 (photoinitiator concentration variation) after polymerisation, 25°C, nematic phase (no field applied).

Polymerisation proceeds even with small amounts of photoinitiator (0.1 wt%) and no differences in texture are observed as the concentration is increased. More surprisingly, polymerisation appears to proceed even in the absence of photoinitiator. Control tests were carried out with another batch of ST03021 and 8CB (same company but different batch numbers), with the same result, ruling out any extrinsic contamination of the chemicals used.

Haze measurements were carried out in the on- and off-states (Figure 16). In both cases, no effect of photoinitiator concentration was noticed, suggesting that the polymer network is not affected by an increase in the photoinitiator concentration. The same conclusions were drawn from a study of the decay times (Figure 17).

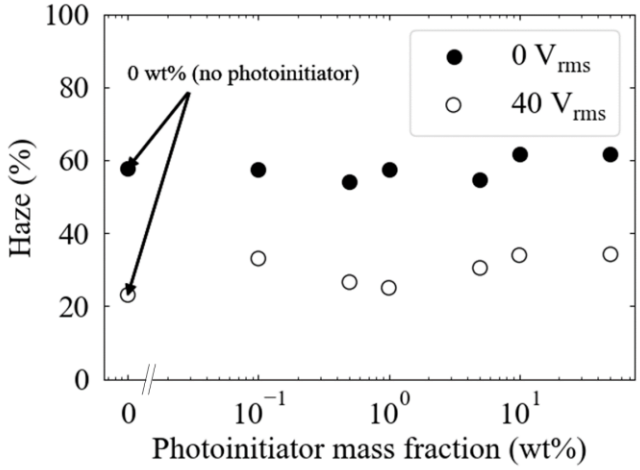

Figure 16: Haze in the off-state (0 V) and the on-state (40 V) versus the photoinitiator mass fraction.

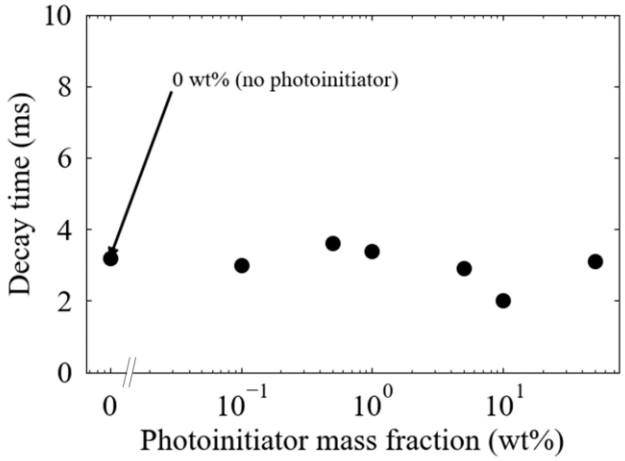

Figure 17: Decay time after a 40 V pulse versus photoinitiator mass fraction (wt%) (series 3, photoinitiator concentration variation).

Polymerised coatings were also prepared to study the morphology of the polymer network as a function of the photoinitiator concentration (Figure 18). No significant differences were observed between the three samples (0 wt%, 2 wt% and 50 wt% photoinitiator).

The effect of photoinitiator concentration on the electro-optical properties of PSLC and the morphology of the polymer networks has not been well described in the literature. Dierking[2] reported no effect of the photoinitiator concentration on the electro-optical properties of PSLC and Li et al.[56] only observed a slight decrease in the distance between polymer walls with increasing photoinitiator concentration, but this behaviour may depend on the chemical nature of the monomer.

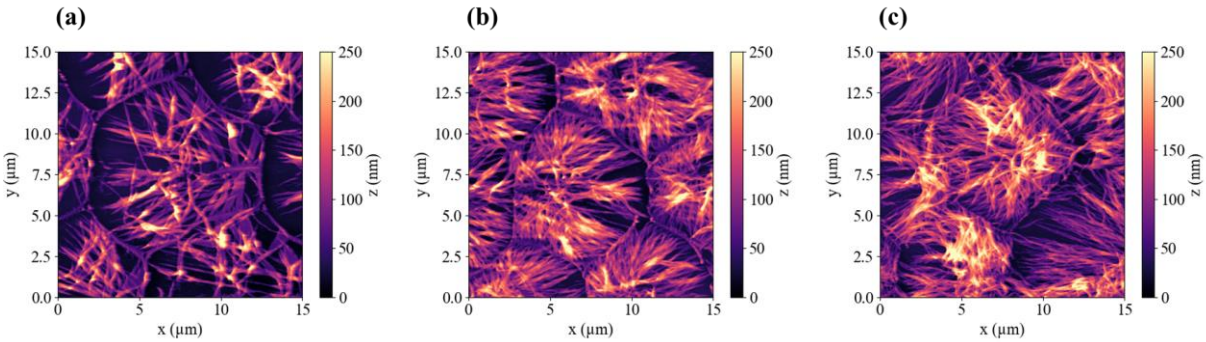

Figure 18: AFM height profiles of washed polymerised coatings. The photoinitiator mass fraction relative to the monomer mass is 0 wt% in (a) 2 wt% in (b) and 50 wt% in (c). In both cases, the reactive mixtures contained 2 wt% monomer and the applied UV light intensity was 16.5 mW/cm².

Since polymerisation seems to proceed in exactly the same way in the absence of a photoinitiator, we assumed that there is an intrinsic impurity in the liquid crystal (for both 8CB and 5CB), as a synthesis by-product that could act as a photoinitiator. Indeed, control experiments (see Suppl. Info. Section 13 for details) showed that the polymerisation occurs in the absence of photoinitiator in 5CB, but not in toluene. To identify the impurity that could act as a photoinitiator, 5CB and 8CB were analysed by LC-MS. Both products were of very high purity rate (5CB: 99.9 % and 8CB: 99.0%).

Nevertheless, the presence of 4-n-octanoylbiphenyl (chemical formula in Figure 19) in 8CB was clearly identified. The details of the analysis are given in SI, part 14. The presence of this molecule in 8CB can be explained by the fact that it may be a by-product of 8CB. An example of 8CB synthesis route and a discussion about the formation of 4-n-octanoylbiphenyl are presented in Figure SI14. Moreover, this molecule is a conjugated ketone and so its formula is very close to type I photoinitiators[57]. Our interpretation of these observations is therefore that the photopolymerisation is initiated by the UV-dissociation of 4-n-octanoylbiphenyl, so that the addition of a photoinitiator (DMPA) may not be necessary. This hypothesis was checked by carrying out photopolymerisation in toluene in the absence of photoinitiator (DMPA) and liquid crystal (8CB and 5CB) but in the presence of 4-n-octanoylbiphenyl (see Figure SI15). We have shown that polymerisation could indeed be initiated by 4-n-octanoylbiphenyl. To our knowledge, this is the first indication that the initiation of photopolymerisation of PSLC systems may be due to an impurity, which obviously requires more detailed studies. Dispensing with the addition of a photoinitiator in the preparation of PSLCs could help to improve their electro-optical properties because some photoinitiators generate ionic impurities when exposed to UV light[58].

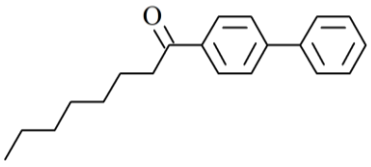

Figure 19: Chemical formula of the impurity, 4-n-octanoylbiphenyl, detected in 8CB.

Conclusions

The kinetics of the polymerisation reaction has been studied by Raman spectroscopy under conditions as close as possible to those of our samples. The polymerisation reaction is probably a first-order reaction and it can be considered complete after 10 minutes of UV exposure.

In the range that we explored, the influence of UV light intensity on the electro-optical properties is very weak but still measurable: as the UV light intensity increases, the haze at 40 V_{rms} increases, the decay time decreases, and the liquid crystal becomes more difficult to align by the electric field. AFM images of the polymer suggest that this is probably because the network is more branched, increasing the contact area between the liquid crystal and the fibres. This could be due to the generation of more radicals in a short time during the initiation step of the polymerisation, but a more detailed study is still needed to prove this point.

The monomer concentration plays a crucial role in the electro-optical properties of the device. The monomer concentration must be between 1 wt% and 5 wt% to retain the defects without exceeding the solubility limit. As the monomer concentration increases, the haze increases in both the on- and off-states. Moreover, AFM images showed that the polymer network becomes denser, although the fibre diameter does not change. The contact area between the polymer fibres and the liquid crystal increases with increasing monomer concentration, and the liquid crystal becomes more difficult to align and scatters more light. In addition, the decay time decreases as the monomer concentration increases and we propose that these two quantities are simply related by $\tau_0 =$

$4\gamma_1 {r_0}^2/(\pi^2 cK)$. The fit of the decay times with this formula confirmed the order of magnitude of the fibre diameter found by AFM.

The influence of the photoinitiator concentration on the electro-optical properties was also investigated, but no effect was found. Surprisingly, the polymerisation worked even without photoinitiator in 8CB, which is a liquid crystal commonly used for PSLC. We tentatively explained this observation by the presence of an impurity in the liquid crystal that could generate radicals and initiate the reaction, but further work is needed to confirm this hypothesis.

From another point of view, this work provided a unique opportunity to visualise the director field in focal conic domains thanks to AFM images of the polymer network. This could help to better understand the structure of these topological defects, which are not only at the basis of this smart window application, but are also ubiquitous in smectic phases.

Acknowledgements:

We would like to thank Emmanuel Garre for his invaluable help with the experimental work and his many suggestions on sample preparation and characterisation. We thank Hanane Belghit for discussions on photoinitiators and LC-HRMS experiments, Anaïs Verron for SEM experiments, Bertrand Heurtefeu and Stéphane Lohou for discussions on polymer chemistry, Cécile Ozanam, Iryna Gozhyk and Laurent Maillaud for discussions on optical measurements, Axel Fouques for discussions on material characterisation, and Olivier Delrieu for measurements of the intensity of UV-lamps. This work was funded by a joint Ph.D. grant from Agence Nationale Recherche et Technologie and Saint-Gobain Research Paris. The authors thank the French Agence Nationale de la Recherche (grant number ANR-23-CE24-0006-03, project DISPLAY) for financial support.

F.M., I.D., C.M. and P.D. designed the project, I.D., C.M. and P.D. supervised it, and C.N.M. performed the experiments and analysed the data which was interpreted by all the authors. C.N.M. prepared the figures and wrote the initial draft of the manuscript which was edited and reviewed by all the authors.

References

(1) Drzaic, P. S. Polymer Dispersed Nematic Liquid Crystal for Large Area Displays and Light Valves. 1986, pp 2142–2148.

(2) Dierking, I. Polymer Network–Stabilized Liquid Crystals. *Advanced Materials* **2000**, *12* (3), 167–181. https://doi.org/10.1002/(SICI)1521-4095(200002)12:3<167::AID-ADMA167>3.0.CO;2-I.

(3) Hikmet, R. a. M. Electrically Induced Light Scattering from Anisotropic Gels. *Journal of Applied Physics* **1990**, *68* (9), 4406–4412. https://doi.org/10.1063/1.346190.

(4) Crawford, G. P.; Zumer, S. *Liquid Crystals In Complex Geometries: Formed by Polymer And Porous Networks*; CRC Press, 1996.

(5) Dierking, I. *Polymer-Modified Liquid Crystals*; Royal Society of Chemistry, 2019.

(6) Yang, D.-K.; Chien, L.-C.; Doane, J. W. Cholesteric Liquid Crystal/Polymer Dispersion for Haze-free Light Shutters. *Appl. Phys. Lett.* **1992**, *60* (25), 3102–3104. https://doi.org/10.1063/1.106765.

(7) Hikmet, R. a. M.; Kemperman, H. Electrically Switchable Mirrors and Optical Components Made from Liquid-Crystal Gels. *Nature* **1998**, *392* (6675), 476–479. https://doi.org/10.1038/33110.

(8) Hu, X.; Zeng, W.; Yang, W.; Xiao, L.; De Haan, L. T.; Zhao, W.; Li, N.; Shui, L.; Zhou, G. Effective Electrically Tunable Infrared Reflectors Based on Polymer Stabilised Cholesteric Liquid Crystals. *Liquid Crystals* **2018**.

(9) Lee, S. N.; Chien, L.-C.; Sprunt, S. Polymer-Stabilized Diffraction Gratings from Cholesteric Liquid Crystals. *SID Symposium Digest of Technical Papers* **1998**, *29* (1), 834–837. https://doi.org/10.1889/1.1833893.

(10) Lu, Y.; Du, F.; Lin, Y.-H.; Wu, S.-T. Variable Optical Attenuator Based on Polymer Stabilized Twisted Nematic Liquid Crystal. *Opt. Express, OE* **2004**, *12* (7), 1221–1227. https://doi.org/10.1364/OPEX.12.001221.

(11) Wu, J.-B.; Wu, S.-B.; Cao, H.-M.; Chen, Q.-M.; Lu, Y.-Q.; Hu, W. Electrically Tunable Microlens Array Enabled by Polymer-Stabilized Smectic Hierarchical Architectures. *Advanced Optical Materials* **2022**, *10* (20), 2201015. https://doi.org/10.1002/adom.202201015.

(12) Sasaki, Y.; Ueda, M.; Le, K. V.; Amano, R.; Sakane, S.; Fujii, S.; Araoka, F.; Orihara, H. Polymer-Stabilized Micropixelated Liquid Crystals with Tunable Optical Properties Fabricated by Double Templating. *Advanced Materials* **2017**, *29* (37), 1703054. https://doi.org/10.1002/adma.201703054.

(13) Kim, J.-H.; Huh, J.-W.; Oh, S.-W.; Ji, S.-M.; Jo, Y.-S.; Yu, B.-H.; Yoon, T.-H. Bistable Switching between Homeotropic and Focal-Conic States in an Ion-Doped Chiral Nematic Liquid Crystal Cell. *Opt. Express, OE* **2017**, *25* (23), 29180–29188. https://doi.org/10.1364/OE.25.029180.

(14) Li, X.; Guo, Y.; Huai, H.; Yang, Y.; Sun, Y.; Zhang, C.; Sun, Y. The Effect of Monomer and Chiral Dopant Content on Reverse-Mode Polymer Stabilized Cholesteric Liquid Crystal Display. *Journal of Molecular Liquids* **2020**, *309*, 113112. https://doi.org/10.1016/j.molliq.2020.113112.

(15) Pan, G.; Cao, Y.; Guo, R.; Cheng, H.; Yang, Z.; Guo, J.; Liang, X.; Zhang, D.; Cao, H.; Yang, H. Effects of the Preparing Condition of a Polymer-Stabilised Liquid Crystal with a Smectic-A−chiral Nematic Phase Transition on Its Properties. *Liquid Crystals* **2009**, *36* (2), 165–172. https://doi.org/10.1080/02678290902752132.

(16) Hu, X.; Zhang, X.; Yang, W.; Jiang, X.-F.; Jiang, X.; Haan, L. T. de; Yuan, D.; Zhao, W.; Zheng, N.; Jin, M.; et al. Stable and Scalable Smart Window Based on Polymer Stabilized Liquid Crystals. *Journal of Applied Polymer Science* **2020**, *137* (30), 48917. https://doi.org/10.1002/app.48917.
(17) Boniello, G.; Vilchez, V.; Garre, E.; Mondiot, F. Making Smectic Defect Patterns Electrically Reversible and Dynamically Tunable Using In Situ Polymer-Templated Nematic Liquid Crystals. *Macromolecular Rapid Communications* **2021**, *42* (11), 2100087. https://doi.org/10.1002/marc.202100087.
(18) Rajaram, C. V.; Hudson, S. D.; Chien, L. C. Effect of Polymerization Temperature on the Morphology and Electrooptic Properties of Polymer-Stabilized Liquid Crystals. *Chem. Mater.* **1996**, *8* (10), 2451–2460. https://doi.org/10.1021/cm9505207.
(19) Guymon, C. A.; Hoggan, E. N.; Clark, N. A.; Rieker, T. P.; Walba, D. M.; Bowman, C. N. Effects of Monomer Structure on Their Organization and Polymerization in a Smectic Liquid Crystal. *Science* **1997**. https://doi.org/10.1126/science.275.5296.57.
(20) Kyongok Kang, L. C. C.; Sprunt, S. Polymer-Stabilized Cholesteric Liquid Crystal Micrograting: A Comparison of Polymer Network Formation and Electro-Optic Properties for Mesogenic and Non-Mesogenic Monomers. *Liquid Crystals* **2002**, *29* (1), 9–18. https://doi.org/10.1080/02678290110093732.
(21) D. F. Gu, A. M. J.; Chien, L. C. Dynamic Light Scattering Study of Polymer-Stabilized Liquid Crystal Monodomain. *Molecular Crystals and Liquid Crystals Science and Technology. Section A. Molecular Crystals and Liquid Crystals* **1996**, *287* (1), 295–304. https://doi.org/10.1080/10587259608038766.
(22) Jákli, A.; Bata, L.; Fodor-csorba, K.; Rosta, L.; Noirez, L. Structure of Polymer Networks Dispersed in Liquid Crystals: Small Angle Neutron Scattering Study. *Liquid Crystals* **1994**, *17* (2), 227–234. https://doi.org/10.1080/02678299408036562.
(23) Jakli, A.; Kim, D. R.; Chien, L.-C.; Saupe, A. Effect of a Polymer Network on the Alignment and the Rotational Viscosity of a Nematic Liquid Crystal. *J. Appl. Phys.* **1992**, *72*, 3161–3164.
(24) Fung, Y. K.; Borstnik, A.; Zumer, S.; Yang, D.-K.; Doane, J. W. Pretransitional Nematic Ordering in Liquid Crystals with Dispersed Polymer Networks. *Phys. Rev. E* **1997**, *55* (2), 1637–1645. https://doi.org/10.1103/PhysRevE.55.1637.
(25) Kraig, R. E.; Taylor, P. L.; Ma, R.; Yang, D.-K. Nematic Order in Polymer-Stabilized Liquid Crystals. *Phys. Rev. E* **1998**, *58* (4), 4594–4597. https://doi.org/10.1103/PhysRevE.58.4594.
(26) Kossyrev, P. A.; Qi, J.; Priezjev, N. V.; Pelcovits, R. A.; Crawford, G. P. Virtual Surfaces, Director Domains, and the Fréedericksz Transition in Polymer-Stabilized Nematic Liquid Crystals. *Appl. Phys. Lett.* **2002**, *81* (16), 2986–2988.
(27) Yang, D.-K.; Cui, Y.; Nemati, H.; Zhou, X.; Moheghi, A. Modeling Aligning Effect of Polymer Network in Polymer Stabilized Nematic Liquid Crystals. *J. Appl. Phys.* **2013**, *114* (24). https://doi.org/10.1063/1.4856295.
(28) Broer, D.; Crawford, G. P.; Zumer, S. *Cross-Linked Liquid Crystalline Systems: From Rigid Polymer Networks to Elastomers*; CRC Press, 2011.
(29) Mondiot, F. Dispositif Electrocommandable a Diffusion Variable Par Cristaux Liquides et Son Procede. FR3086771A1, April 3, 2020.
(30) Meyer, C.; Jonckheere, B.; Penaud, C. The Construction of the Dupin Cyclides in a Smectic A Polygonal Texture. *Journal of Materials* **2014**, *2014*, e145375. https://doi.org/10.1155/2014/145375.

(31) Zappone, B.; Meyer, C.; Bruno, L.; Lacaze, E. Periodic Lattices of Frustrated Focal Conic Defect Domains in Smectic Liquid Crystal Films. *Soft Matter* **2012**, *8* (16), 4318–4326. https://doi.org/10.1039/C2SM07207F.
(32) Gim, M.-J.; Beller, D. A.; Yoon, D. K. Morphogenesis of Liquid Crystal Topological Defects during the Nematic-Smectic A Phase Transition. *Nature Communications* **2017**, *8* (1), 1–9. https://doi.org/10.1038/ncomms15453.
(33) RAJARAM, C. V.; HUDSON, S. D.; CHIEN, L. C. Morphology of Polymer-Stabilized Liquid Crystals. *Chem. mater* **1995**, *7* (12), 2300–2308.
(34) I. DIERKING, A. C. L., L. L. KOSBAR; HELD, G. A. Polymer Network Structure and Electro-Optic Performance of Polymer Stabilized Cholesteric Textures II. The Effect of UV Curing Conditions. *Liquid Crystals* **1998**, *24* (3), 397–406. https://doi.org/10.1080/026782998207217.
(35) Anseth, K. S.; Wang, C. M.; Bowman, C. N. Reaction Behaviour and Kinetic Constants for Photopolymerizations of Multi(Meth)Acrylate Monomers. *Polymer* **1994**, *35* (15), 3243–3250. https://doi.org/10.1016/0032-3861(94)90129-5.
(36) Colthup, N. B.; Daly, L. H.; Wiberley, S. E. *Introduction to Infrared and Raman Spectroscopy*; Elsevier, 1990.
(37) McCormick, D. T.; Chavers, R.; Guymon, C. A. Investigation of Polymer Nanostructure Evolution during the Formation of Polymer/Smectic Liquid Crystal Composites. *Macromolecules* **2001**, *34* (20), 6929–6935. https://doi.org/10.1021/ma010571r.
(38) Guymon, C. A.; Bowman, C. N. Polymerization Behavior and Kinetics during the Formation of Polymer-Stabilized Ferroelectric Liquid Crystals. *Macromolecules* **1997**, *30* (6), 1594–1600. https://doi.org/10.1021/ma9616773.
(39) Courtecuisse, F.; Karasu, F.; Allonas, X.; Croutxé-Barghorn, C.; van der Ven, L. Confocal Raman Microscopy Study of Several Factors Known to Influence the Oxygen Inhibition of Acrylate Photopolymerization under LED. *Progress in Organic Coatings* **2016**, *92*, 1–7. https://doi.org/10.1016/j.porgcoat.2015.11.020.
(40) Scherzer, T.; Decker, U. Kinetic Investigations on the UV-Induced Photopolymerization of a Diacrylate by Time-Resolved FTIR Spectroscopy: The Influence of Photoinitiator Concentration, Light Intensity and Temperature. *Radiation Physics and Chemistry* **1999**, *55* (5), 615–619. https://doi.org/10.1016/S0969-806X(99)00257-1.
(41) Wall, B. G.; Koenig, J. L. Studying the Curing Kinetics of a Diacrylate by Using Infrared Spectroscopy. *Appl Spectrosc* **1997**, *51* (10), 1453–1459. https://doi.org/10.1366/0003702971939181.
(42) Oh, S. J.; Lee, S. C.; Park, S. Y. Photopolymerization and Photobleaching of N-Butyl Acrylate/Fumed Silica Composites Monitored by Real Time FTIR-ATR Spectroscopy. *Vibrational Spectroscopy* **2006**, *42* (2), 273–277. https://doi.org/10.1016/j.vibspec.2006.05.028.
(43) Fung, Y. K.; Yang, D.-K.; Ying, S.; Chien, L.-C.; Zumer, S.; Doane, J. W. Polymer Networks Formed in Liquid Crystals. *Liquid Crystals* **1995**, *19* (6), 797–801. https://doi.org/10.1080/02678299508031102.
(44) Panov, V. P.; Song, J.-K.; Mehl, G. H.; Vij, J. K. The Beauty of Twist-Bend Nematic Phase: Fast Switching Domains, First Order Fréedericksz Transition and a Hierarchy of Structures. *Crystals* **2021**, *11* (6), 621. https://doi.org/10.3390/cryst11060621.
(45) Ma, R.-Q.; Yang, D.-K. Freedericksz Transition in Polymer-Stabilized Nematic Liquid Crystals. *Phys. Rev. E* **2000**, *61* (2), 1567–1573. https://doi.org/10.1103/PhysRevE.61.1567.

(46) Dessaud, N.; Raynes, P.; Bonnett, P. Dielectric Behavior of Polymer-Stabilized-Liquid-Crystal Cells Made from Hosts with Different Ultraviolet Absorptions. *J. Appl. Phys.* **2004**, *96* (8), 4366–4371. https://doi.org/10.1063/1.1790589.
(47) Baek, J.-I.; Kim, K.-H.; Kim, J. C.; Yoon, T.-H.; Woo, H. S.; Shin, S. T.; Souk, J. H. Fast Switching of Vertical Alignment Liquid Crystal Cells with Liquid Crystalline Polymer Networks. *Jpn. J. Appl. Phys.* **2009**, *48* (5R), 056507. https://doi.org/10.1143/JJAP.48.056507.
(48) Hikmet, R. A. M.; Boots, H. M. J. Domain Structure and Switching Behavior of Anisotropic Gels. *Phys. Rev. E* **1995**, *51* (6), 5824–5831. https://doi.org/10.1103/PhysRevE.51.5824.
(49) Ilk Capar, M.; Cebe, E. Rotational Viscosity in Liquid Crystals: A Molecular Dynamics Study. *Chemical Physics Letters* **2005**, *407* (4), 454–459. https://doi.org/10.1016/j.cplett.2005.03.125.
(50) Cui, M.; Kelly, J. R. Temperature Dependence of Visco-Elastic Properties of 5CB. *Molecular Crystals and Liquid Crystals Science and Technology. Section A. Molecular Crystals and Liquid Crystals* **1999**, *331* (1), 49–57. https://doi.org/10.1080/10587259908047499.
(51) Chatopadhayay, P.; Roy, S. K. Splay and Bend Elastic Constants in 7CB and 8CB. *Molecular Crystals and Liquid Crystals Science and Technology. Section A. Molecular Crystals and Liquid Crystals* **1994**, *257* (1), 89–98. https://doi.org/10.1080/10587259408033766.
(52) Sun, J.; Wang, H.; Wang, L.; Cao, H.; Xie, H.; Luo, X.; Xiao, J.; Ding, H.; Yang, Z.; Yang, H. Preparation and Thermo-Optical Characteristics of a Smart Polymer-Stabilized Liquid Crystal Thin Film Based on Smectic A–Chiral Nematic Phase Transition. *Smart Mater. Struct.* **2014**, *23* (12), 125038. https://doi.org/10.1088/0964-1726/23/12/125038.
(53) Dierking, I.; Kosbar, L. L.; Afzali-Ardakani, A.; Lowe, A. C.; Held, G. A. Two-Stage Switching Behavior of Polymer Stabilized Cholesteric Textures. *J. Appl. Phys.* **1997**, *81* (7), 3007–3014. https://doi.org/10.1063/1.364335.
(54) Sergan, V.; Sergan, T.; Dozov, I.; Joly, S.; Voss, R. Orientational Order Induced by a Polymer Network in the Isotropic Phase of Liquid Crystal. *Phys. Rev. E* **2020**, *101* (5), 052705. https://doi.org/10.1103/PhysRevE.101.052705.
(55) Li, X.; Guo, Y.; Huai, H.; Yang, Y.; Sun, Y.; Zhang, C.; Sun, Y. The Effect of Monomer and Chiral Dopant Content on Reverse-Mode Polymer Stabilized Cholesteric Liquid Crystal Display. *Journal of Molecular Liquids* **2020**, *309*, 113112. https://doi.org/10.1016/j.molliq.2020.113112.
(56) Li, L.; Catanescu, C. O.; Chien, L.-C. Dynamics of Phase Separation and Morphology of Polymer Stabilized Liquid Crystals. In *Emerging Liquid Crystal Technologies III*; SPIE, 2008; Vol. 6911, pp 133–140. https://doi.org/10.1117/12.767379.
(57) Green, W. A. *Industrial Photoinitiators: A Technical Guide*; CRC Press, 2010.
(58) Lee, K. M.; Tondiglia, V. P.; Godman, N. P.; Middleton, C. M.; White, T. J. Blue-Shifting Tuning of the Selective Reflection of Polymer Stabilized Cholesteric Liquid Crystals. *Soft Matter* **2017**, *13* (35), 5842–5848. https://doi.org/10.1039/C7SM01190C.